Experimental Study of Stark Broadening of the Allowed and Forbidden Transitions $2\,^3P$-$4\,^3D$, $4\,^3F$ ($\lambda = 4471.5$ Å, $\lambda = 4470$ Å) in Neutral Helium

H. W. Drawin and J. Ramette

Association EURATOM-CEA, Département de la Physique du Plasma et de la Fusion Contrôlée, Centre d'Etudes Nucléaires, Boîte Postale n° 6, 92 Fontenay-aux-Roses (France)

(Z. Naturforsch. **29 a**, 838–850 [1974] ; received July 3, 1973 *)

Measurements were made of the profile of the HeI 4471.5 Å line and its forbidden component at $\lambda = 4469.9$ Å, emitted from an afterglow plasma of electron densities in the range 2.2×10^{14} to 1.5×10^{15} cm^{-3}. The various quantities which define position and form of the profile have been compared with the theoretical calculations of Griem and of Barnard et al. It has been found that the wavelength shifts of the individual components and, thus, the peak separation are slightly smaller than predicted by theory, whereas the intensity in the valley between the two components is found to be slightly larger than the theoretical values. The peak intensity of the forbidden component is smaller than given by theory but not as small as found by D. D. Burgess and C. J. Cairns. At low electron densities the intensity of the forbidden component is proportional to the square of the normal field strength F_0 of the electric microfield. At higher electron densities the intensity increases proportionally to F_0 in agreement with the transition from quadratic to linear Stark effect at higher electric field strengths. The measurements show that the influence of the ion dynamics on the line profile is probably not as large as assumed by D. D. Burgess. The measurements show that the position of the intensity minimum between allowed and forbidden component is shifted towards the allowed component when the temperature decreases.

Introduction

The broadening of the $\lambda = 4471.5$ Å spectral line of neutral helium and its forbidden component situated at $\lambda = 4469.9$ Å has been object of several theoretical and experimental studies due to its special importance in the diagnostics of laboratory and astrophysical plasmas and in the calculation of model star atmospheres. The first theoretical study has been published by Unsöld [1], see also [2]. In this study, the displacement of the upper levels $4\,^3P$ and $4\,^3F$ has been obtained from the average value of the electric microfield of the perturbing plasma ions in connection with the already earlier determined displacements in a static electric field (Foster [3], Foster and Douglas [4]), whereas the broadening was calculated using the impact approximation of Lindholm [5] and Foley [6] with H^+ ions as the only perturbers (the most abundant ionic species in stellar atmospheres to which the calculations were applied). Unsöld neglected broadening due to electronic collisions. These latter ones were accounted for by Griem [7] and independently by Barnard, Cooper and Shamey [8]. Both papers are based on the calculation technique of Baranger [9], Kolb and Griem [10], and Griem, Baranger, Kolb and Oertel [11]: The broadening due to the ions is treated in the quasi-static approximation, the impact approximation is applied to the broadening due to the electron collisions. The calculations of Griem [7] and Bernard et al. [8] show very similar results as far as the gross structure of the line profile is concerned, in certain wavelength regions, however, the numerical values deviate considerably from each other. Brissaud and Frisch [12a, b] developed a method which accounts simultaneously for quasi-static ion broadening, electronic impact broadening and approximately for ion-dynamical broadening. As far as the HeI $\lambda = 4471.5$ Å line is concerned detailed profile calculations are not yet available for the range of electron densities investigated in the present paper.

The broadening of the $\lambda = 4471.5$ Å line has been measured by several authors at very different electron densities (see Table I). The first study was by Wulff [13] who measured the broadening for an electron density of 3×10^{16} cm^{-3}. Systematic experimental studies of the line profile began only a few years ago and immediately after the publication of the theoretical calculations of Griem and Barnard et al. who listed their results for a wide range of electron density n_e and temperature T in a convenient form including convolution with a Doppler

* Revised version received March 7, 1974.
Reprint requests to Dr. H. W. Drawin, Association EURATOM-CEA, Département de la Physique du Plasma et de la Fusion Contrôlée, Boîte Postale n° 6, *F-92 Fontenay-aux-Roses*, Frankreich.

Table 1. Experimental studies of the broadening of the He I $\lambda = 4471.5$ Å line and its forbidden component.

Author(s)	Year	n_e [cm^{-3}]	T_e [°K]	Experiment
Wulff [13]	1958	3×10^{16}	4.4×10^{4}	flash tube, pulsed arc
Birkeland et al. [14]	1971	$4\times10^{15}\ldots2\times10^{16}$	$1\times10^{4}\ldots2\times10^{4}$	vortex stabilized d. c. arc
Burgess and Cairns [15]	1970 1971	$4\times10^{14}\ldots1\times10^{15}$	$5\times10^{3}\ldots1.3\times10^{4}$	Z-pinch, observation during afterglow
Jenkins and Burgess [16]	1971	$1.2\times10^{16}\ldots3\times10^{16}$	$4\times10^{4}\ldots5\times10^{4}$	Z-pinch; observation during compression
Nelson and Barnard [17]	1971	$3\times10^{16}\ldots1\times10^{17}$	$\approx 4.5\times10^{4}$	flash tube pulsed arc; observation during maximum current
Diatta and Chapelle [18]	1972	2.7×10^{16}	1.8×10^{4}	plasma jet; observation in afterglow region
Baravian et al. [19]	1973	$4.2\times10^{16}\ldots1.8\times10^{17}$	$2\times10^{4}\ldots4\times10^{4}$	laser produced plasma; observation during afterglow
Present work	1973	$2.2\times10^{14}\ldots1.5\times10^{15}$	$3.4\times10^{3}\ldots6.3\times10^{3}$	flash tube, pulsed arc; observation during afterglow

profile (the temperature of the emitters was assumed to be equal to the electron temperature, a hypothesis often not fulfilled in laboratory plasmas).

Comparison of measured profiles with the theoretical calculations showed the following features: In general, the measured line contours are in relatively good agreement with the theoretical ones as far as the gross structure of the profile is concerned. However, disagreement between theory and measurements exists in the "fine structure" of the profiles: At high electron densities Birkeland et al. [14] and Nelson and Barnard [17] measured a smaller wavelength separation between the allowed and forbidden component than predicted by theory, and the minimum between both components was less pronounced than for the theoretical profiles. Whereas Birkeland [14] et al. still observed at $n_e = 1\times10^{17}$ cm^{-3}, Nelson and Barnard [17] at $n_e = 4.5\times10^{16}$ cm^{-3}, and Diatta and Chapelle [18] at $n_e = 2.7\times10^{16}$ cm^{-3} a well-pronounced intensity minimum between allowed and forbidden components in agreement with theory, no such minimum was observed by Jenkins and Burgess [16] for electron densities equal to and larger than 1×10^{16} cm^{-3}. This latter result is thus in serious contradiction to the theoretical results not only of Griem [7] and of Barnard et al. [8] but also to those of Brissaud [12c] who also found a well-pronounced intensity minimum at these high electron densities.

At low electron densities the only existing experimental results are those of Burgess and Cairns [15] who measured in the center of the forbidden component much lower and in the dip between allowed and forbidden component slightly larger intensities than the theoretically calculated ones. Moreover, the measured peak separation both components was slightly larger than predicted by theory. Also the intensity in the (violet) line wing of the forbidden component appeared to be much higher than the calculated intensities.

At present, the agreement between measurements made by different authors as well as the agreement between experimental and theoretical results is less than satisfactory, either at high or at low electron densities. We therefore set up an experiment in order to determine the line profile of the $2\,^3P - 4\,^3D$, $4\,^3F$ transitions by using a specially designed 10-channel spectrum analyzer. We have concentrated our efforts on the determination of the line profile at low electron densities (see Table 1).

Experimental

1. Discharge Tube, Electrical Circuit

The linear discharge tube had an effective length of 32 cm and an inner diameter of 30 mm. The electrodes at both ends were coated with tungsten and had a central boring of 20 mm diameter closed by plane quartz windows. The shot-to-shot reproductibility of the light emission both as a function of time and of space could considerably be improved by illuminating the cathode surface uniformly with UV radiation delivered by a high-pressure mercury lamp. After evacuation to 10^{-7} torr during several days the tube was filled with pure helium (filling pressure 4 torr for all measurements).

The discharge was powered by a 10 KV, 3 μF capacitor triggered via an ignitron. The plasma current was limited by a $R = 4.5\ \Omega$ resistance. In order to ensure identical plasma conditions for all shots the plasma current and the light intensity were monitored simultaneously. The corresponding signals were storaged on an oscilloscope screen. The intensity of the He I $\lambda = 5876$ Å line served as the monitor signal for the light emitted from the plasma.

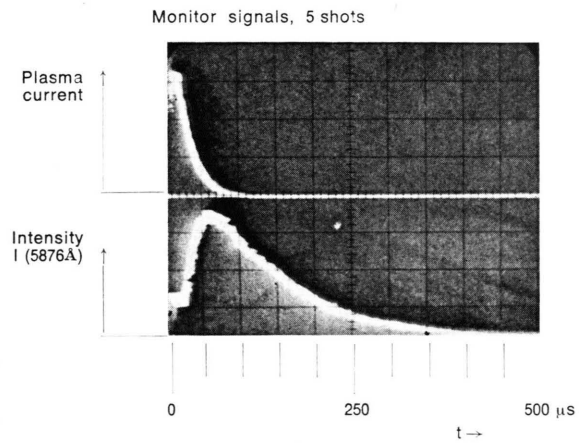

Fig. 1. Discharge current (upper trace) and intensity of the HeI $\lambda = 5876$ Å line (lower trace) as a function of time. Five successive shots superposed. The current peak corresponds to 750 A at 24 μs. Time base: 50 μs/div.

Figure 1 shows the plasma current (upper trace) and the intensity of the $\lambda = 5876$ Å line (lower trace) as a function of time. Five successive shots have been superposed. The maximum current was 750 A at 24 μs. At 150 μs the current was still 20 A, and at 250 μs a residual current of approximately 3 to 4 A could still be measured.

Electron density, electron temperature and line profiles have been obtained by observing the plasma "end-on" in its axial region.

2. Determination of Electron Density

Electron densities in the region of the discharge axis were determined using a He-Ne (mono-mode) laser interferometer system after Ashby and Jephcott [20]. The $\lambda = 3.39\ \mu$ radiation served for probing the plasma, the change of the optical refractivity (which is practically only determined by the number of free electrons) has been detected by observing the modulation of the intensity of the $\lambda = 6329$ Å line as a function of time. In order to improve the detection sensitivity during the late afterglow we have increased the path length by a factor three using two additional reflection mirrors. One interference fringe then corresponds to a change in the electron density of $3.4 \times 10^{14}\ \mathrm{cm}^{-3}$. We consider half of this value as the lowest detectable density in our experiment, with a precision of $\pm 25\%$ owing to the well-known difficulties in fixing the zero point at the end of the afterglow.

3. Determination of Electron Temperature

The electron temperature T_e has been determined from the relative population densities of highly excited He I levels (Boltzmann plot). The latter ones have been obtained from the simultaneously measured intensities (in relative units) of ten spectral lines displayed in two spectral bands in the focal plane of a Bausch and Lomb dual-grating 2 m Ebert type spectrograph. The light was captured by ten light-guide systems (made from quartz fibers for the lines in the UV) and detected by means of ten photomultipliers the out-put voltages of which were displaced on ten oscilloscop screens. The sensitivity of the detectors relative to each other has been determined by means of chopped light emitted by either a tungsten ribbon and a jodin-halide lamp (Manufacturer: Optics Technology, Palo Alto/California, U.S.A.).

It was thus possible to measure simultaneously the time history of ten spectral intensities during the same shot. By displacing the receivers in the focal plan we also determined the continuum intensity in the vicinity of the lines. For times later than 30 μs the continuum intensity was negligibly small (less than 1%) compared to the line intensities. Figure 2

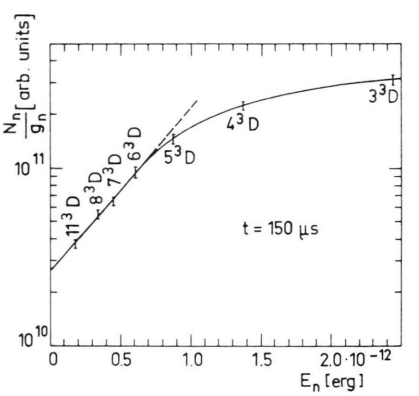

Fig. 2. Measured population densities N_n (in relative units) divided by the statistical weight $g_n = 15$ of the n^{3}D-levels of HeI as a function of ionization energy E_n at time $t = 150\ \mu$s.

shows as an example the measured population densities N_n (divided by the statistical weight $g_n = 15$) of seven n^{3}D levels as obtained from the observation of seven lines of the $2\,^3\mathrm{P} - \mathrm{n}^3\mathrm{D}$ spectral series at time $t = 150\ \mu$s. Strong deviations from partial

L.T.E. occur for quantum levels $n=3$ and 4. The straight line which connects the measured values for $5 \leqq n \leqq 11$ as a function of ionization energy E_n yields in this special case an electron temperature of $T_e = 3500\ ^\circ\mathrm{K}$ ($\pm 250\ ^\circ\mathrm{K}$).

Only light from a small region around the discharge axis passed through the entrance slit of the spectrograph. Electron density and electron temperature of the observed region are given in Figure 3. (The temporal evolution of the light intensity

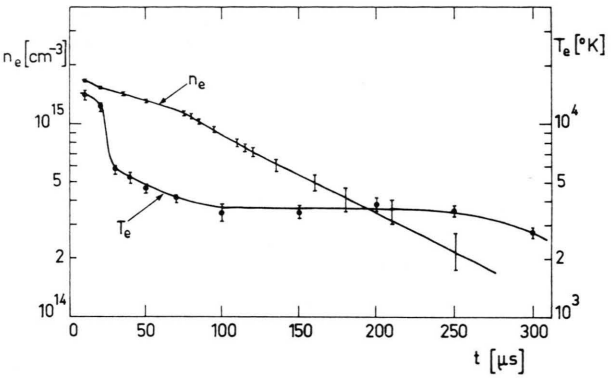

Fig. 3. Temporal evolution of electron temperature T_e and electron density n_e during the afterglow phase.

is shown in Figure 1.) One sees that the electron density decreases continuously with time whereas the electron temperature stays nearly constant from 80 μs to 240 μs. Two reasons are responsible for this effect. First: During the recombination phase superelastic electronic collisions heat the electrons, and second: The low residual current of a few amperes which is still flowing (20 A at 150 μs, 3 to 4 A at 250 μs) represents an additional source of heating. Both effects together compensate the energy losses due to heat conduction and radiation and maintain the electron temperature at an elevated level.

4. Gas Temperature

The gas temperature has not been measured. Since energy is continuously fed into the free electron gas due to superelastic collisions and also due to slight heating by a residual electric current of several amperes, the electron temperature will surely stay above the temperature of the heavy particles. Fortunately, both the radial diffusion lengths to the walls and the time during which T_e remains constant favours the energy exchange between electrons and heavy particles and hence the relaxation to a commun temperature. One can therefore expect that the gas temperature T_g takes values which are not too different from T_e at least for times later than 100 μs after the break-down. Since the electrons are continuously heated by superelastic collisions and by the residual current mentioned above the inequality $T_e > T_g$ holds during the whole afterglow.

5. Measurement of Line Profiles, 10-Channel Analyzer

A special 10-channel system has been built for observing simultaneously the intensities within the line profile in ten closely spaced wavelength bands. The receiving head consisted of ten parallel rows of glass fibers (each of diameter 100 μ), the total width being $10 \times 100\ \mu = 1.0$ mm. The height of each row is 30 mm (which has only partly been used in the present experiment).

The fibers of each row formed a light guide which was connected to the photocathode of a photomultiplier (Philips 56 UVP). The ten out-put voltages were displaced on ten oscilloscop screens.

In stead of placing the receiving head in the focal plan of the spectrograph we have magnified a small region of the focal plan by means of a highly corrected lens and then placed the receiver in this new plane (see Figure 4). Imaging system and receiving head were mounted on a support which could separately be moved parallel to the focal plane and the receiving head itself was additionally movable in three dimensions. It was thus possible to focalise a spectral line on the receiving head and to aligne the rows parallel to this line. Our system is similar to the 9-channel analyzer system of Baravian et al.[21].

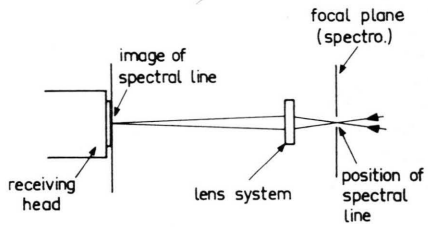

Fig. 4. Position of the 10-channel analyzer system (receiving head) relative to the focal plane of the spectrograph.

All measurements have been performed with the above mentioned Bausch and Lomb spectrograph. The line profiles were analyzed using a grating with 1200 lines/mm. At $\lambda = 4470$ Å the measured dispersion was equal to 0.25 mm/Å in the focal plane of the spectrograph. Since the focal plane appeared 4 times magnified in the plane of the receiving head, a resolution of 0.1 Å per channel was obtained.

The sensitivity of each channel has been measured by illuminating the entrance slit with the chopped continuous radiation of a tungsten ribbon lamp. The spectral emissivity has been assumed to be constant

over the wavelength region of 1 Å covered by the 10 channels. The linearity light intensity-out put voltage has also been checked.

The position of the unperturbed transition $2\,^3P - 4\,^3D$ at $\lambda = 4471.48$ Å has been determined by means of a low-pressure He discharge ($n_e \lesssim 10^{12}$ cm^{-3}). It was thus possible to observe the change of the position of the allowed line during the afterglow relative to the unperturbed position at $\lambda = 4471.48$ Å.

The complete line profiles have been obtained as follows: First, the receiving head was put in such a position that the maximum of the (unperturbed) allowed line emitted by the low-pressure lamp fell on the limit of two adjacent rows and that both channels gave the same out-put signal. By moving the receiving head slightly to the left and the right the signal of one channel decreases for the benefit of the other. It was thus possible to fixe the position of the wavelength $\lambda = 4471.48$ Å with a precision of ± 0.01 Å.

Immediately after this procedure the low-pressure lamp has been removed and the light emitted by the decaying high-pressure plasma was observed "end-on" and the oscilloscop traces of the ten photomultiplier out-put signals were photographed. The receiving head has then be displaced in steps of 0.5 mm to the left and to the right and the measurement of the light signals repeated. The measurements were made with different oscilloscop sensitivities in order to ensure optimum deflection and reading of the oscilloscop traces at different times of the afterglow.

Results, Comparison with Theory

1. General

Some measured line profiles are shown in Figs. 5 to 9 for different values of n_e and T_e. They are compared with theoretical profiles calculated by Griem [7] and Barnard et al. [8]. All profiles are normalized to unity according to the relation:

$$\underset{\text{allowed component}}{\int} I_a(\lambda)\,d\lambda + \underset{\text{forbidden component}}{\int} I_f(\lambda)\,d\lambda = 1\,. \qquad (1)$$

The theoretical calculations have only been performed for a limited number of electron densities and very few temperatures. Therefore an interpolation routine had to be applied in order to get theoretical profiles for plasma parameters others than directly calculated. This interpolation poses principal difficulties due to the fact that in the theoretical calculations electron and gas temperatures have been assumed to be equal whereas in our experiment the gas temperature is surely smaller than the electron temperature. Further, for the lowest electron densities measured, the measured electron temperatures lie slightly below the lowest temperature for which the theoretical calculations have been performed ($T \geqq 5000$ °K). Therefore the theoretical values should be extrapolated to lower temperatures. This extrapolation procedure is not without danger, since one introduces errors depending on the kind the extrapolation is performed. Fortunately an extrapolation procedure turned out to be unnecessary as may be seen from Fig. 10 which shows the theoretical line profile for $n_e = 3.45 \cdot 10^{14}$ cm^{-3} (inter-

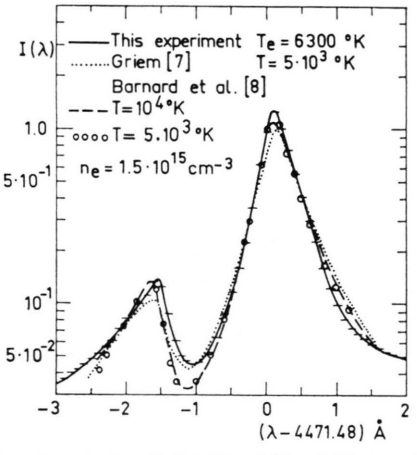

Fig. 5. Profile of the HeI $2\,^3P - 4\,^3D$, $4\,^3F$ transition for $n_e = 1.5 \times 10^{15}$ cm^{-3} ($\pm 3\%$). The horizontal lines of width 0.1 Å indicate the measured intensities of the individual channels.

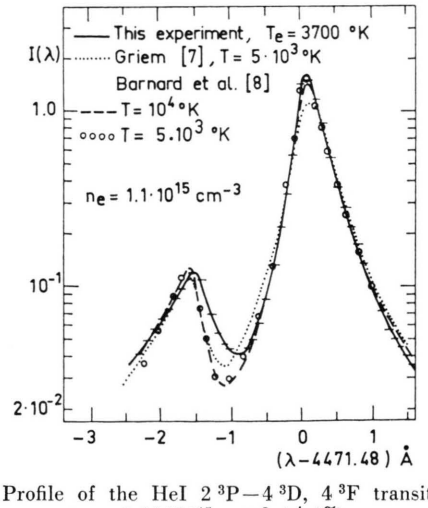

Fig. 6. Profile of the HeI $2\,^3P - 4\,^3D$, $4\,^3F$ transition for $n_e = 1.1 \times 10^{15}$ cm^{-3} ($\pm 4\%$).

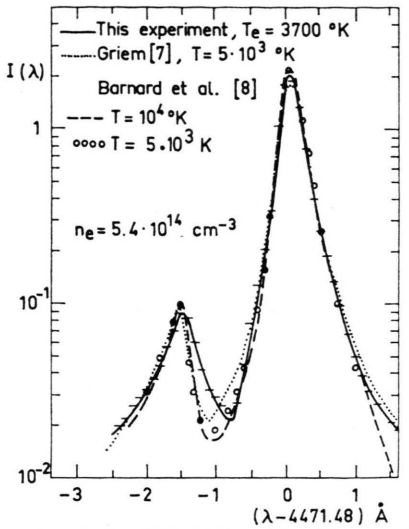

Fig. 7. Profile of the HeI $2\,^3P-4\,^3D$, $4\,^3F$ transition for $n_e = 5.4\times10^{14}\,\mathrm{cm}^{-3}$ ($\pm 8\%$).

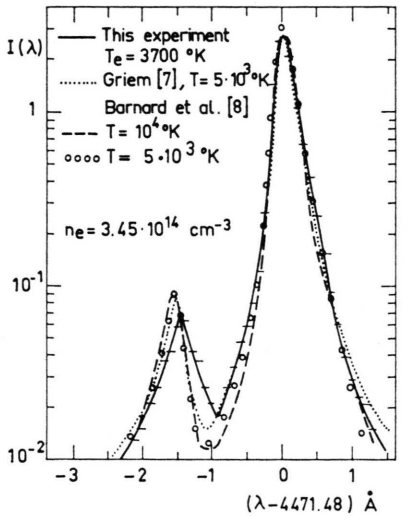

Fig. 8. Profile of the HeI $2\,^3P-4\,^3P-4\,^3F$ transition for $n_e = 3.45\times10^{14}\,\mathrm{cm}^{-3}$ ($\pm 12\%$).

polated) at a temperature of $T = 5000\,^\circ\mathrm{K}$ for which Griem [7] has tabulated theoretical values. We have then extrapolated the theoretical values to $T = 3700\,^\circ\mathrm{K}$ (which corresponds to our measured electron temperature). The corresponding "theoretical" profile is also shown in Figure 10. The two profiles are nearly identical, a slight difference occurs in the region of the minimum between allowed and forbidden component: Decreasing temperature increases the line intensity and shifts the minimum slightly towards the allowed component. Such a shift has been observed experimentally (see Figs. 5 to 9), but it is much larger than theory predicts.

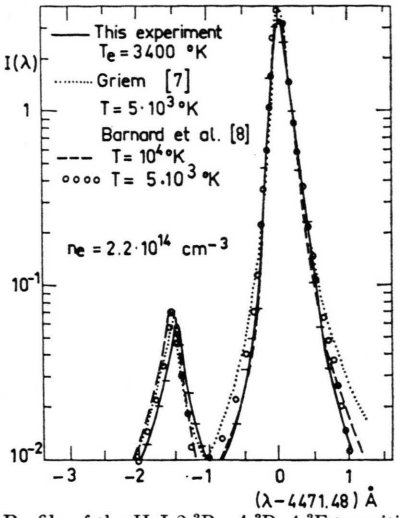

Fig. 9. Profile of the HeI $2\,^3P-4\,^3D$, $4\,^3F$ transition for $n_e = 2.2\times10^{14}\,\mathrm{cm}^{-3}$ ($\pm 20\%$).

The measured profiles are compared with the theoretical profiles of Griem [7] for $T = T_e = T_i = T_{gas} = 5000\,^\circ\mathrm{K}$ and with those of Barnard et al. [8] for $T = 10^4\,^\circ\mathrm{K}$ and $5000\,^\circ\mathrm{K}$. It should be mentioned that the listed theoretical values contain already convolution with the corresponding Doppler profiles.

The theoretical profiles should principally be convolved with the instrumental profile prior to comparison with measurements, or one should unfold the measured profiles. Two main instrumental broadening effects have to be distinguished:

i) Modification of the true profile due to instrumental broadening of the spectrograph (mainly broadening due to slit width). The (full) half width of a Cd line ($\lambda = 4414.63$ Å) emitted from a low pressure discharge lamp, was $\Delta\lambda_A \cong 0.12$ Å in the focal plane of the spectrograph. This value can be considered as the half width of the apparatus profile of the spectrograph, since the line width of the Cd line is much smaller than the width of the apparatus profile.

ii) An additional modification of the line profile due to imperfectnesses of the 10-channel analyzer system:
   - a – Eventual modification of the line profile when it is transmitted from the focal plane of the spectrograph onto the measuring head containing the ten rows of glass fibers (image errors).
   - b – Imperfect alignment of the rows of the measuring head.
   - c – Light leaks between adjacent channels.

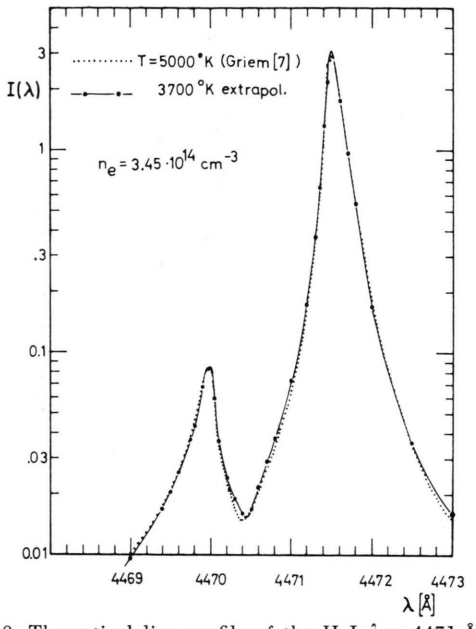

Fig. 10. Theoretical line profile of the HeI $\lambda = 4471$ Å line after Griem [7] for $n_e = 3.45 \times 10^{14}$ cm^{-3}. The curve for $T = 3700$ °K has been obtained by extrapolating the theoretical values to lower temperatures.

Measurement of the intensity distribution of the above mentioned Cd line led to the following relative intensity distribution over the 10 channels: Central channel (located on line maximum), relative intensity = 100; the two adjacent channels to the left and right, intensity (in each) = 15 ± 2; the third channel (to the left and right) gave an intensity $\cong 2$. The contributions of channels farther away appears to be insignificant and are not distinguishable from noise. Thus, we assume that the overall instrumental profile is decreasing monotonically from the line center. This intensity distribution corresponds practically to the one of the apparatus profile of the spectrograph when cut in ten equivalent wavelength intervals. It follows from this that the analyzer system itself does not modify notably the line profile, the modification is due mainly to the apparatus function of the spectrograph. Thus, only the influence of the latter has to be discussed.

Two physical situations must be distinguished:

1) At the higher electron densities the influence of the instrumental profile on the line contour is in any case negligibly small, as can directly be seen when comparing the widths of the total profiles with that of the apparatus function.

2) At the lowest electron densities measured the instrumental profile would have an influence on the profiles mainly in the central part of the rather sharp allowed component provided the experimental temperatures were identical with those for which Doppler folding has been undertaken in the mentioned theoretical papers. However, the gas temperatures in the experiment are smaller than the ones assumed in the theoretical work. Under the present conditions the apparatus function of the spectrograph has approximately the same effect on the experimental profile than the Doppler folding procedure in the theoretical calculation of the line profiles.

Indeed, the theoretical profiles contain Doppler broadening for gas temperatures of 10^4 °K and 5000 °K, the corresponding Doppler widths of the He $\lambda = 4471$ Å line are $\Delta\lambda_D = 0.16$ Å and $\Delta\lambda_D = 0.11$ Å respectively. At the end of the afterglow, the gas temperature will probably not exceed 2500 °K. The corresponding Doppler width is 0.078 Å. Since the Doppler widths enter quadratically in the folding procedure, the experimental profiles are less affected by Doppler effect than the theoretical calculations made for the higher temperatures. An additional folding of the theoretical line profiles with the apparatus function would therefore lead to an overestimation of the theoretical broadening compared to the actual experimental situation. It is much better to compare directly the measured profiles (with apparatus broadening included) with the theoretical profiles containing Doppler broadening (for the higher temperatures) but no folding with the apparatus function. The comparison between experiment and theory has finally been made in this way. Compared to the theoretical profiles this procedure leads to an overestimate of the experimental broadening which can in any case not be larger than $A - B = 0.075$ Å where

$$A = \Delta\lambda_A + \Delta\lambda_D(\text{theor}) \left[\frac{\Delta\lambda\,(\text{exp})}{\Delta\lambda_D\,(\text{theor})} \right]^2$$

denotes the width of an experimental profile only broadened due to instrumental ($\Delta\lambda_A$) and Doppler effects ($\Delta\lambda_D(\text{exp})$), the latter relative to the Doppler effect assumed in the theoretical work ($\Delta\lambda_D(\text{theor})$), whereas $B = \Delta\lambda_D(\text{theor})$ is the width of a (hypothetical) theoretical line broadened by Doppler effect alone. With $T(\text{theor}) = 5000$ °K, $T(\text{exp}) = 2500$ °K and $\Delta\lambda_A = 0.12$ Å one obtains $+0.075$ Å which is three-fourth of a channel width. Since the lines are additionally broadened by Stark effect the absolute error should be somewhat smaller than this value.

In each figure we have indicated the intensity of each channel together with the channel width (equal to 0.1 Å). The heading of each figure gives the plasma parameters to which the different profiles refer.

Figure 11 is a schematic representation of the He I $\lambda = 4471.5$ Å line profile and indicates the various parameters which are discussed below.

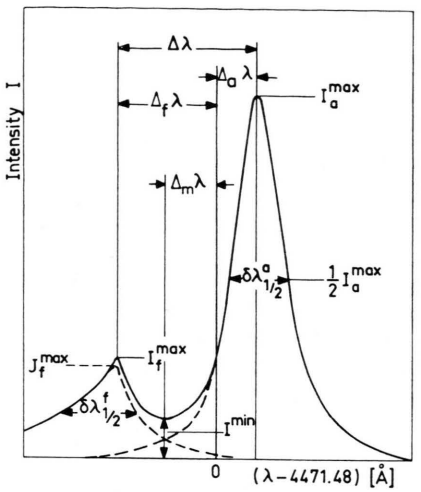

Fig. 11. Schematic representation of the profile of the $\lambda = 4471.5$ Å line and its forbidden component.

2. *Gross Structure of Line Profiles*

The measurements show an intense allowed line accompanied by a much weaker component which originates from the forbidden transition $2\,^3P - 4\,^3F$ induced by the electric field of the charged plasma particles. The general structure of the line contours is well described by the theoretical calculations. Especially the intensity distribution in the red wing of the allowed component shows relatively good agreement between experiment and theory, but agreement is not as good as found by Burgess and Cairns [15]. One further sees that in our measurements the forbidden component is much more peaked and the valley between allowed and forbidden component is deeper than in the measurements of Burgess and Cairns (which may be due partly to the lower temperatures and the higher resolution in the present work). At the higher electron densities ($n_e = 1.5 \times 10^{15}$ cm^{-3} to $n_e = 5.4 \times 10^{14}$ cm^{-3}) our measured intensities in the vicinity of the maximum of the forbidden component agree especially well with the theoretical calculations of Barnard et al. [8] A sizeable discrepancy discovered by Burgess and Cairns for the same electron density but higher temperatures ($T = 13\,000$ °K, see their Fig. 3) has not been found in the present work.

With decreasing electron density (and thus with decreasing electron temperature) one finds a characteristic displacement of the minimum between allowed and forbidden components, which cannot be explained by a temperature effect (see Fig. 10) in the existing theories. In view of the earlier discussion of instrumental errors, this effect appears to be a real feature.

The peak separation is not as large as predicted by theory.

The different parameters defining the profile shall be discussed in more detail.

3. *Wavelength Shift and Peak Separation*

The interaction of charged plasma particles and emitters shifts the energy levels of the latter ones and, thus, the wavelengths of the spectral lines. The shift increases with the density of charged particles. As far as the He I $2\,^3P - 4\,^3D$, $4\,^3F$ transitions are concerned the allowed component is shifted to longer wavelengths whereas the forbidden line is shifted to the blue. We have measured the wavelength distances $\Delta_a\lambda$ and $\Delta_f\lambda$ (for notation, see Fig. 11) from the position of the unperturbed wavelength of the allowed line and, thus, the total wavelength separation $\Delta\lambda = |\Delta_a\lambda| + |\Delta_f\lambda|$ of the intensity maxima of

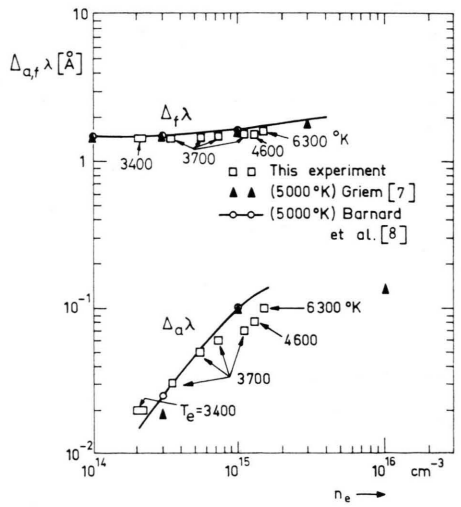

Fig. 12. Wavelength shift of the allowed ($\Delta_a\lambda$) and the forbidden ($\Delta_f\lambda$) component as a function of electron density. The measured electron temperatures are indicated as a parameter.

the two lines during the recombination phase. Figure 12 shows the measured values of $\Delta_a\lambda$ and $\Delta_f\lambda$ together with the theoretical predictions. The experiment yields slightly smaller wavelength shifts than the theory.

The total wavelength separation $\Delta\lambda$ is shown in Figures 13 a, b. Figure 13 a gives a comparison of theory with experiments at low electron densities.

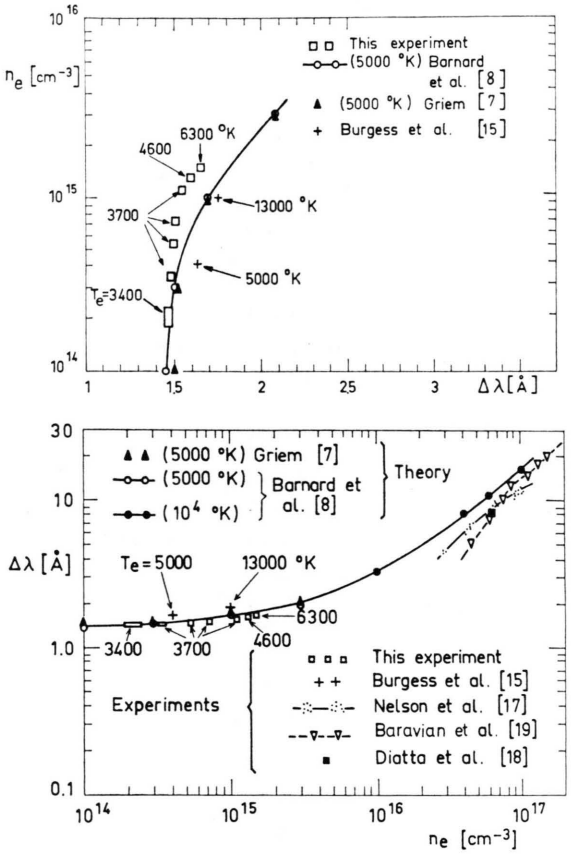

Fig. 13. Peak separation $\Delta\lambda = |\Delta_a\lambda| + |\Delta_f\lambda|$. a— Present measurements compared with the measurements of Burgess and Cairns [15] and the theoretical calculations of Griem [7] and Barnard et al. [8]. b— Comparison of all known experimental values with the theoretical predictions of Griem [7] and Barnard et al. [8].

The theoretical values lie between our measured values and those of Burgess and Cairns [15]. For decreasing electron densities our measurements yield peak separation which tend well to the limiting value for low electron densities as calculated by Barnard et al. [8]. (Theoretical value: $\Delta\lambda = 1.46$ Å for $n_e = 1\times10^{14}$ cm^{-3}; measured value: $\Delta\lambda = 1.47 \pm 0.01$ Å for $n_e = 2.2\times10^{14}$ cm^{-3}.) The value of $\Delta\lambda = 1.50$ Å at $n_e = 1\times10^{14}$ cm^{-3} calculated by Griem [7] seems to be too large. The rather large wavelength separations of the two peaks as measured by Burgess and Cairns [15] could not be confirmed.

Figure 13 b shows a comparison of the theoretically predicted peak separation with all recently published values with the exception of those measured by Birkeland et al. [14]. These authors indicated some uncertainty of the absolute wavelength calibration of the monochromator used for the measurements. With the exception of the measurements of Burgess and Cairns [15] all experimentally determined values are smaller than the theoretically calculated peak separations. No experimental values are known for the intermediate electron density range $2\times10^{15} \leqq n_e\,[\mathrm{cm}^{-3}] \leqq 2\times10^{16}$.

4. Peak Intensities, Intensity of the Valley

Figure 14 shows the measured peak intensities of the allowed (I_a^{max}) and the forbidden line (I_f^{max}) and the minimum intensity (I^{min}) in the valley between both components compared with the theoretically calculated values.

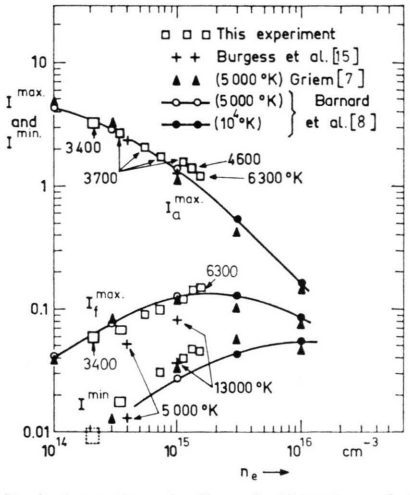

Fig. 14. Peak intensity of allowed (I_a^{max}) and forbidden (I_f^{max}) component and intensity I^{min} of the valley between the two components. The measured electron temperatures are given as a parameter.

For the allowed line the measured peak intensities agree remarkably well with the theoretical values for $n_e < 1\times10^{15}$ cm^{-3}. For $n_e > 1\times10^{15}$ cm^{-3}, the experimental values lie slightly above the theoretical ones.

The agreement between theory and measurements is less good for the peak intensity of the forbidden component. For $n_e \lesssim 1\times10^{15}$ cm^{-3}, the measured

values lie definitely below the theoretical ones. For $n_e > 10^{15}$ cm^{-3}, however, the situation is reversed: For $n_e = 1.3 \times 10^{15}$ and 1.5×10^{15} cm^{-3} the measured values lie slightly above the theoretical predictions. It should be pointed out, however, that the temperatures for the experimental and theoretical values are not exactly the same. In the electron density range about 10^{15} cm^{-3} – where all plasma parameters are closest to those for which the theoretical calculations have been performed – good agreement is found between theory and experiment. The behaviour of the measured values can partly be explained by an "electron temperature effect": Impact broadening due to electronic collisions is proportional to $T_e^{-1/2}$. For given electron density the profile will become broader for decreasing electron temperature. Since normalization is conserved, the peak intensity decreases. For T_e increasing, the contrary holds. Although our temperatures are lower than those of Burgess and Cairns [15] we did not find peak intensities I_f^{max} as low as those measured by these authors. It follows from our measurements that ion dynamics is probably less important than initially assumed by Burgess [22]. Our experimental results are partly confirmed by the recent calculations of Lee [23] and Ségré and Voslamber [24].

The largest discrepancy between theory and experiment is found for the minimum intensity I^{min} of the valley between forbidden and allowed line. All measured values lie clearly above the theoretical ones. The same discrepancy between theory and experiment has been found by other authors at higher electron densities. At low electron densities, Burgess and Cairns [15] measured minimum intensities at two electron densities. For $n_e = 10^{15}$ cm^{-3} and $T_e = 13000$ °K (see cross + in Fig. 14) their value agrees well with our ones for $n_e = 1.1 \times 10^{15}$ cm^{-3} and $T_e = 3700$ °K. For $n_e = 4 \times 10^{14}$ cm^{-3} and $T_e = 5000$ °K their measured intensity value lies just between the theoretical values of Griem [7] and Barnard et al. [8] in contrast to the present study which yields minimum intensities which all lie well above the theoretical ones both of Griem and Barnard et al.

5. Position of Minimum Intensity

The measurements show a characteristic shift with electron density and, thus, with electron temperature of the position of the minimum intensity between allowed and forbidden components. For the electron density $n_e = 1.5 \times 10^{15}$ cm^{-3} the measured position agrees still well with the theoretical one (see Figure 5). With decreasing electron density the calculated profiles show a very slight shift of the minimum towards the allowed line, but the shift is not so pronounced as for the measured profiles. The measurements indicate that the position of the intensity minimum is much more sensitive to temperature than to density in the electron density range treated here.

6. Half-widths of Allowed and Forbidden Component

The width of the allowed line at one-half of the maximum intensity is easy to measure. The measured values are shown in Fig. 15 together with the values of other authors. At low electron densities

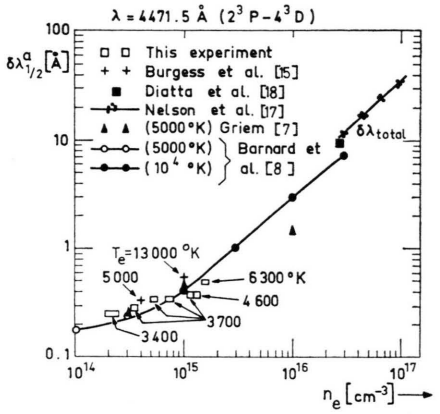

Fig. 15. Full half width $\delta\lambda^a_{1/2}$ of the allowed component $\lambda = 4471.5$ Å. At high electron densities the total half width $\delta\lambda_{total}$ of the allowed and forbidden components together is given.

our half-widths are smaller than those calculated by Griem [7] but they agree rather well with those of Barnard et al. [8] except for electron densities $n_e > 10^{15}$ cm^{-3} where they are somewhat smaller.

At high electron densities the half-width of the allowed line is not further well defined due to merging of the allowed and forbidden component. We have therefore indicated the total width of both components at one-half of the maximum intensity of the allowed line ($\delta\lambda_{total}$ in Figure 15).

The half-width of the forbidden line is difficult to determine due to partial merging of the two components even at rather low electron densities. In order to obtain an approximate value we have em-

pirically separated the intensity values into two contributions, one belonging to the forbidden and the other one belonging to the allowed line. This is indicated by the broken curves in Figure 11. The sum of the individual intensities of both lines yields for each wavelength the intensity of the composed profile. This procedure yields now for the (isolated) forbidden line a modified peak intensity (J_f^{max} in Figure 11). The width at one-half of this value is the half-width of the (isolated) forbidden component. The corresponding values are shown in Fig. 16 together with the values predicted by theory which obviously yields too small half-widths.

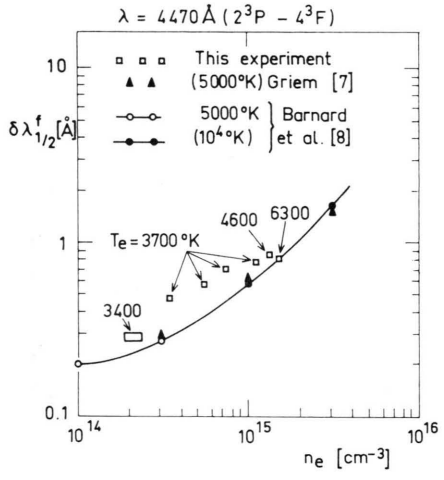

Fig. 16. Full half width $\delta\lambda^f_{1/2}$ of the forbidden component.

7. *Ratio of Line Intensities*

The decomposition into two individual line profiles permits now the determination of the intensity contained in each component. Of special interest is the knowledge of the intensity contained in the forbidden transition $2\,^3P - 4\,^3F$ relative to the sum of the intensities of the allowed and forbidden transitions. This intensity ratio can be written as follow

$$R = \frac{\int\limits_{\text{forbidden line}} I_f(\lambda)\,d\lambda}{\int\limits_{\text{allowed line}} I_a(\lambda)\,d\lambda + \int\limits_{\text{forbidden line}} I_f(\lambda)\,d\lambda} = \int\limits_{\text{forbidden line}} I_f(\lambda)\,d\lambda \tag{2}$$

due to the normalization condition (1).

The ratio R as obtained from the measured line profiles is shown in Fig. 17 as a function of the measured electron density n_e. At low values of n_e the intensity contained in the forbidden component is

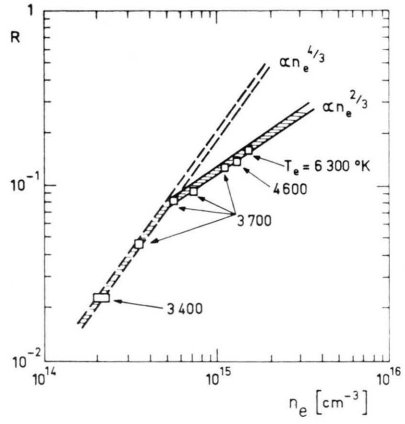

Fig. 17. Intensity ratio R as a function of electron density n_e. The measured electron temperatures have been indicated as a parameter.

(within the experimental error bars) proportional to $n_e^{4/3}$. With increasing electron density the slope becomes smaller. For $n_e > 5 \times 10^{14}$ cm^{-3} the increase of R with n_e is proportional to $n_e^{2/3}$. Since the normal field strength F_0 of the electric microfield is given by

$$F_0 = 2.603\, e_0\, n_e^{2/3} \tag{3}$$

we obtain the following laws:

– for low electron densities ($n_e < 5 \times 10^{14}$ cm^{-3}):

$$R = 1.1 \times 10^{-3} F_0^2 \ (\pm 15\%) \tag{4}$$

– for high electron densities ($n_e > 5 \times 10^{14}$ cm^{-3}):

$$R = 0.93 \times 10^{-2} F_0 \ (\pm 15\%) \tag{5}$$

where F_0 is in electrost. cgs units. At very high electron densities R will approach the asymptotic value 0.5, since the same amount of energy will be contained in both components when complete mixing of the wavefunctions is achieved. The estimated uncertainty of $\pm 15\%$ in relations (4) and (5) is due to the uncertainty in the decomposition of the experimental line profile in two separate profiles. The experimentally determined relations (4) and (5) practically agree with the relations found by Foster and Douglas [3, 4] for static Stark effect when F_0 is replaced by the static electric field strength F.

Conclusion

Line profiles of the HeI transitions $2\,^3P - 4\,^3D$, $4\,^3F$ have been measured for the electron density range $2.2 \times 10^{14} \leqq n_e[\text{cm}^{-3}] \leqq 1.5 \times 10^{15}$. A summary of the measured quantities which define the

Table 2. Summary of the experimental results.

t [μs]	n_e [10^{14} cm^{-3}]	T_e [°K]	I_a^{max}	I_f^{max}	I^{min}	$\Delta_a\lambda$ [Å]	$\Delta_f\lambda$ [Å]	$\Delta\lambda$ [Å]	$\Delta_m\lambda$ [Å]	$\delta\lambda_{1/2}^a$ [Å]	$\delta\lambda_{1/2}^f$ [Å]	R	R^*
25	15 ± 3%	6300	1.27	0.14	0.047	+0.1	−1.55	1.65	−1.1	0.47	0.80	0.160	0.184
50	13 ± 3%	4600	1.44	0.13	0.045	+0.08	−1.50	1.58	−1.0	0.37	0.86	0.146	0.166
80	11 ± 4%	3700	1.58	0.12	0.041	+0.07	−1.47	1.54	−0.9	0.37	0.77	0.122	0.140
120	7.2 ± 6%	3700	1.72	0.10	0.032	+0.06	−1.45	1.51	−0.9	0.33	0.70	0.0902	0.100
150	5.4 ± 8%	3700	2.08	0.09	0.021	+0.05	−1.45	1.50	−0.9	0.33	0.58	0.0810	0.084
200	3.5 ± 12%	3700	2.70	0.067	0.018	+0.03	−1.45	1.48	−0.9	0.28	0.48	0.0460	0.049
250	2.2 ± 20%	3400	3.20	0.060	≦0.01	+0.02	−1.45	1.47	−0.9	0.25	0.29	0.0225	0.023

profile is given in Table 2. The observed line contours show the general features predicted by the theoretical calculations of Griem [7] and Barnard et al. [8]. In several points, however, the measured intensity distribution deviates from the calculated ones:

i) The wavelength shifts of the allowed and forbidden component and, thus, the peak separation $\Delta\lambda$ are found to be smaller than predicted by theory.

ii) A discrepancy between experiment and theory also exists for the minimum intensity in the valley between the allowed and forbidden line. The measured intensities are larger than the theoretical ones.

iii) The minimum has a smaller wavelength distance from the unperturbed position than predicted by theory.

iiii) The peak intensity of the forbidden component is found to be slightly smaller than the theoretically calculated values, but the large discrepancies between experiment and theory observed by Burgess and Cairns [15] could not be confirmed by the present study. It follows from this that the influence of the ion dynamics on the line profile is probably not as large as supposed by Burgess [22]. Recent calculations of Lee [23] who accounted for the ion dynamics yield for $n_e = 10^{15}$ cm^{-3}, $T = 10^4$ °K a peak intensity which is situated between those of Burgess and Cairns [15] and the present value.

By decomposing the measured profiles into two separate lines – a method which necessarily includes some arbitraryness – it was possible to determine the intensity contained in the forbidden component relative to the total intensity of both lines [ratio R, see Eq. (2)] and relative to the intensity contained in the allowed line only. The measured values of this latter ratio denoted by

$$R^* = \int_{\substack{\text{forbidden}\\ \text{line}}} I_f(\lambda)\,d\lambda \Big/ \int_{\substack{\text{allowed}\\ \text{line}}} I_a(\lambda)\,d\lambda \qquad (6)$$

have also been listed in Table 2.

The measurement yields an increase of the intensity of the forbidden component proportional to the normal field strength F_0 for electron densities larger than 5×10^{14} cm^{-3}. For lower electron densities the intensity is proportional to F_0^2. The transition from one F_0-dependence to the other occurs in a relatively small electron density range situated about 5×10^{14} cm^{-3}. The normal field strength which corresponds to this value agrees well (within a factor two to three) with the static electric field strength for which Foster and Douglas found the transition from quadratic to linear Stark effect.

Inspection of the literature shows that no experiments have yet been performed for electron densities ranging approximately from 2×10^{15} cm^{-3} to 2×10^{16} cm^{-3}. Such measurements would surely be very useful in connection with refined theoretical studies.

Acknowledgements

We would like to thank Mr. E. Sablon for technical assistance and the help during the whole experimental programmes. The assistance of Miss F. Emard is also gratefully acknowledged.

[1] A. Unsöld, Z. Astrophysik **23**, 75 [1944].

[2] A. Unsöld, Physik der Sternatmosphären, 2. Aufl., Springer-Verlag, Berlin-Heidelberg 1955.

[3] J. S. Foster, Proc. Roy. Soc. (London) A **117**, 137 [1927].
[4] J. S. Foster and A. V. Douglas, Monthly Notices **99**, 150 [1939].
[5] E. Lindholm, Ark. f. mat. astr. och Fysik **32** A, 17 [1945].
[6] H. M. Foley, Phys. Rev. **69**, 616 [1946].
[7] H. R. Griem, Astrophys. J. **154**, 1111 [1968].
[8] A. J. Barnard, J. Cooper, and L. J. Shamey, Astron. and Astrophysic **1**, 28 [1969].
[9] M. Baranger, Phys. Rev. **111**, 494 [1958].
[10] A. C. Kolb and H. R. Griem, Phys. Rev. **111**, 514 [1958].
[11] H. R. Griem, M. Baranger, A. C. Kolb, and G. Oertel, Phys. Rev. **125**, 177 [1962].
[12a] U. Frisch and A. Brissaud, J. Quant. Spectr. Radiative Transfer **11**, 1753 [1971].
[12b] A. Brissaud and U. Frisch, J. Quant. Spectr. Radiative Transfer **11**, 1767 [1971].
[12c] A. Brissaud, Thesis, University of Paris (1971).
[13] H. Wulff, Z. Physik **150**, 614 [1958].
[14] J. W. Birkeland, M. E. Bacon, and W. G. Braun, Phys. Rev. A **3**, 354 [1971].
[15] D. D. Burgess and C. J. Cairns, J. Physics B **3**, L. 67 [1970]; J. Physics B **4**, 1364 [1971].
[16] J. E. Jenkins and D. D. Burgess, J. Physics B **4**, 1353 [1971].
[17] R. H. Nelson and A. J. Barnard, J. Quant. Spectr. Radiative Transfer **11**, 161 [1971].
[18] C. S. Diatta and J. Chapelle, to be published.
[19] G. Baravian, J. Bretagne, J. L. Godart, and G. Sultan, to be published.
[20] D. E. T. F. Ashby and D. F. Jephcott, Applied Physics Letters **3**, 13 [1963].
[21] G. Baravian, R. Benattar, J. Bretagne, G. Callede, J. L. Godart, and G. Sultan, Internal report L. P. 108, Laboratoire de Physique des Plasmas, Faculté des Sciences d'Orsay, Université Paris XI [1970].
[22] D. D. Burgess, J. Physics B **3**, L 70 [1970].
[23] R. W. Lee, J. Physics B **5**, L 23 [1972].
[24] E. R. A. Ségré and D. Voslamber, Physics Letters, **46 A** [1974], to be published.